Research Square

Preprints are preliminary reports that have not undergone peer review.
They should not be considered conclusive, used to inform clinical practice,
or referenced by the media as validated information.

Thinning, acceleration and calving of Petermann Glacier, northern Greenland

Kate Briggs

k.briggs@lancaster.ac.uk

Lancaster University https://orcid.org/0009-0009-3007-0951

Malcolm McMillan

Lancaster University https://orcid.org/0000-0002-5113-0177

Anna Hogg

University of Leeds https://orcid.org/0000-0002-6441-4937

Karla Boxall

Lancaster University https://orcid.org/0000-0002-6574-7717

Adam Garbo

University of Ottawa https://orcid.org/0000-0002-7312-7390

Anna Crawford

University of Stirling https://orcid.org/0000-0003-3620-1130

Molly Hammond

University of Leeds https://orcid.org/0000-0002-8511-2911

Benjamin Wallis

School of Earth, Environment and Sustainability, University of Leeds https://orcid.org/0000-0003-3671-2862

Clare Willis

Lancaster University

Iain Wheel

University of Stirling

Jennifer Maddalena

University of Lancaster

Amber Leeson

Lancaster University https://orcid.org/0000-0001-8720-9808

Joe Phillips

University of Lancaster

Article

Keywords:

Posted Date: July 15th, 2026

DOI: https://doi.org/10.21203/rs.3.rs-10140188/v1

License: This work is licensed under a Creative Commons Attribution 4.0 International License.
Read Full License

Additional Declarations: There is **NO** Competing Interest.

Thinning, acceleration and calving of Petermann Glacier, northern Greenland

Briggs, K. H.[1*], McMillan, M.[1], Hogg, A. E.[2], Boxall, K.[1], Garbo, A.[3], Crawford, A. J.[4], Hammond, M. A.[2], Wallis, B. J.[2], Willis, C.[1], Wheel, I.[4], Maddelena, J. [1], Leeson, A.[1] and Phillips, J.[1]

[1]UK Centre for Polar Observation and Modelling, Centre of Excellence in Environmental Data Science, Lancaster Environment Centre, Lancaster University, Lancaster, United Kingdom

[2] School of Earth, Environment and Sustainability, University of Leeds, Leeds, United Kingdom

[3] Department of Geography, Environment and Geomatics, University of Ottawa, Ottawa, Canada.

[4] Division of Biological and Environmental Sciences, University of Stirling, Stirling, United Kingdom.

Abstract

Petermann Glacier drains 6% of the Greenland Ice Sheet and contains sufficient ice to raise global sea level by 0.41 m. Terminating in one of five remaining ice shelves in Greenland, it has been considered historically stable, with little evidence of a sustained response to changes in its surrounding climate. Here, we use a suite of satellite observations to document decadal-scale ice shelf thinning and acceleration, alongside the development of a major calving event. Following the rapid propagation of a rift across the ice shelf during the past two summers, the ice shelf is now poised to lose 22% of its area, leaving the calving front at its most receded position since observational records began. We show that the recent thinning of the ice shelf occurred during a period of anomalously warm upper ocean waters and substantially reduced landfast sea ice at the mouth of Petermann Fjord. Inland glacier acceleration is now detectable more than 50 km upstream of the glacier's grounding line, indicating the emergence of a dynamic imbalance at one of Greenland's largest marine-terminating glaciers. Our findings highlight the need to better understand the physical mechanisms that will govern Petermann's future evolution and sea level contribution.

Introduction

The Greenland Ice Sheet (GrIS) is the largest ice mass in the Northern Hemisphere, covering an area of ~1.7×10^6 km^2 and containing sufficient ice to raise global mean sea level by ~7.4 m if fully melted[1]. Since the late 20th Century, the GrIS has transitioned from a state of near mass balance, to sustained net mass loss[2, 3], contributing a total of ~14 mm to global sea-level rise over the past three decades[3]. These changes have been

driven by a combination of increased melting of its surface and enhanced ice discharge at its marine-terminating margins[4,5]. Increasing atmospheric temperatures in the Arctic, which have risen two to four times faster than the global mean[6, 7], have driven longer and more intense summer melt seasons, and been accompanied by an increased frequency of extreme melt events[4,8, 9]. Concurrently, changes in the surrounding ocean have perturbed the dynamics of many marine-terminating glaciers, as they have responded to increased heat content delivered onto the continental shelf [10, 11, 12]. Declining Arctic sea ice has also modified air-ocean heat exchange which, in turn, has enhanced regional ocean warming[7, 13]. With rapid changes expected in the Arctic climate over the remainder of the 21st century and beyond[7], understanding the physical processes governing the ice sheet's current and future response is central to establishing reliable mass loss, sea-level rise, and climate projections (e.g. [14, 15, 16]). These are important both societally and economically, given the risks that sea-level rise poses to low-lying coastal communities, infrastructure, and ecosystems[17].

At the ice sheet scale, Greenland's mass loss over the past three decades has been due, in approximately equal measures, to surface and dynamical mass imbalance[5, 18, 19]. At the regional scale, however, the relative contribution of these two factors varies considerably, reflecting spatial differences in atmospheric and ocean forcing, alongside glacier and fjord geometry (e.g. [11, 20, 21]). In broad terms, surface processes have dominated the overall observed imbalance in the north, northeast and southwest regions of the ice sheet, whereas dynamical imbalance has dominated in the northwest and southeast[5]. Whilst the impact of increased atmospheric temperatures on surface mass loss is relatively well-understood (e.g. [22, 23]), the complex interactions that govern

the response of marine-terminating glaciers to changes in their surrounding ocean and atmospheric conditions are less well constrained [24, 25, 26]. As a result, the future dynamical response of marine-terminating glaciers remains one of the principal uncertainties in projections of Greenland's future sea level contribution[27, 14]. Nonetheless, recent observations[28] indicate that ocean thermal forcing is the primary driver of ice melt, dynamic thinning and grounding line retreat at many of Greenland's marine-terminating outlet glaciers, with surface melt acting to further amplify the ocean's melt potential[26].

Of particular importance to understanding the ice sheet's future evolution is the stability of the floating ice shelves that remain at the termini of five of Greenland's major outlet glaciers[29, 30]. Combined, these five glaciers contain almost 20% of Greenland's total sea-level rise equivalent[30]. Their floating extensions – which are sometimes referred to as ice tongues – have the capacity to restrain inland ice flow through the transmission of resistive stresses upstream [30, 31], and also to generate large, tabular icebergs via episodic calving. Thus, their evolution impacts both the grounded ice sheet, and the downstream fjord and ocean environments. Weakening, thinning and retreat of these ice shelves may reduce their buttressing effect, leading to acceleration, dynamic thinning, and increased ice discharge from some of the largest outlet glaciers that drain the ice sheet [21, 30, 32]. Furthermore, calving of large, tabular icebergs and their subsequent drift, disintegration and melting, delivers solid and liquid freshwater to the ocean, where it may act to alter the surrounding water properties and circulation patterns[33, 34]. These *ice islands*, as they are termed in the Arctic, also represent potential

hazards for commercial shipping, cruise tourism and resource extraction industries [35, 36, 37, 38].

The second largest ice shelf in Greenland is located at the terminus of Petermann Glacier[30]; a major marine-based glacier in northwest Greenland. Petermann Glacier is one of the largest flow features on the ice sheet, draining ~ 6% of the ice sheet by area[39] and holding 1.6×10^5 km^3 of ice volume above flotation; equivalent to a sea-level potential of 0.41 m[40, 41]. The ice shelf currently spans an area of 1,169 km^2 and sits within a confined 15-20 km wide fjord that exits into the Nares Strait, which separates Greenland from Ellesmere Island (Figure 1a). The ice shelf thickness varies from ~150 m near the calving front to ~600 m at the glacier's grounding line[42], where its main trunk rests on bedrock that is approximately 400-500 m below sea level. Recent mass loss from the ice shelf has been dominated (~80%) by basal melting[43, 44], reflecting the presence of relatively warm Atlantic Water in the sub-shelf cavity (e.g. [45, 46]) and the constrained fjord geometry that suppresses calving[44, 47]. Inland of the grounding line, surface meltwater runoff has also been linked to modest seasonal ice speed variability[47, 48]. Taken together, these observations suggest that Petermann Glacier has the capacity to respond to future changes in both oceanic and atmospheric conditions, as the Arctic climate continues to warm.

Historically, Petermann Glacier has been regarded as dynamically stable, with little evidence of sustained change in ice velocity, discharge, or grounding line position in response to past calving events[47]. Although episodic calving has occurred throughout the observational record[49], readvances of the ice shelf in the intervening periods resulted in a broadly stationary calving front position between 1876 and 2010[50]. The

most recent large calving events, that occurred in August 2010 and July 2012 were, however, unprecedented in scale, removing 293 km^2 and 137 km^2 of floating ice respectively[34], and leaving the terminus at its most retreated position since observations began[49]. Despite the magnitude of these losses however, the dynamic response of the glacier was observed to be transient, with short-lived velocity increases of approximately 10–12%[47, 51, 52], and limited migration of the grounding line[53]. The lack of a significant response was attributed to the small resistive stresses exerted by the distal ice shelf relative to the driving forces acting at the grounded ice; a consequence of its relatively thin geometry, weak lateral attachment to the fjord walls, and rheologically soft ice towards the calving front[47, 54].

Despite these observations, the extent to which Petermann Glacier will remain stable in the face of ongoing changes to its surrounding climate remains an open question. The ice shelf has lost nearly half of its surface area over the past 16 years, and recent modelling suggests that if this trajectory continues, future breakup may be irreversible[29], which would likely have significant implications for future sea-level rise. Indeed, recent observations have indicated a period of grounding line retreat between 2017 and 2021, leading to suggestions that Petermann Glacier may already be transitioning into a phase of dynamic destabilisation[55]. Here, we use a suite of satellite observations to track the development of a major calving event on the Petermann Ice Shelf, and to assess evidence for sustained and widespread ice shelf thinning, acceleration and dynamic imbalance over the past decade.

Results

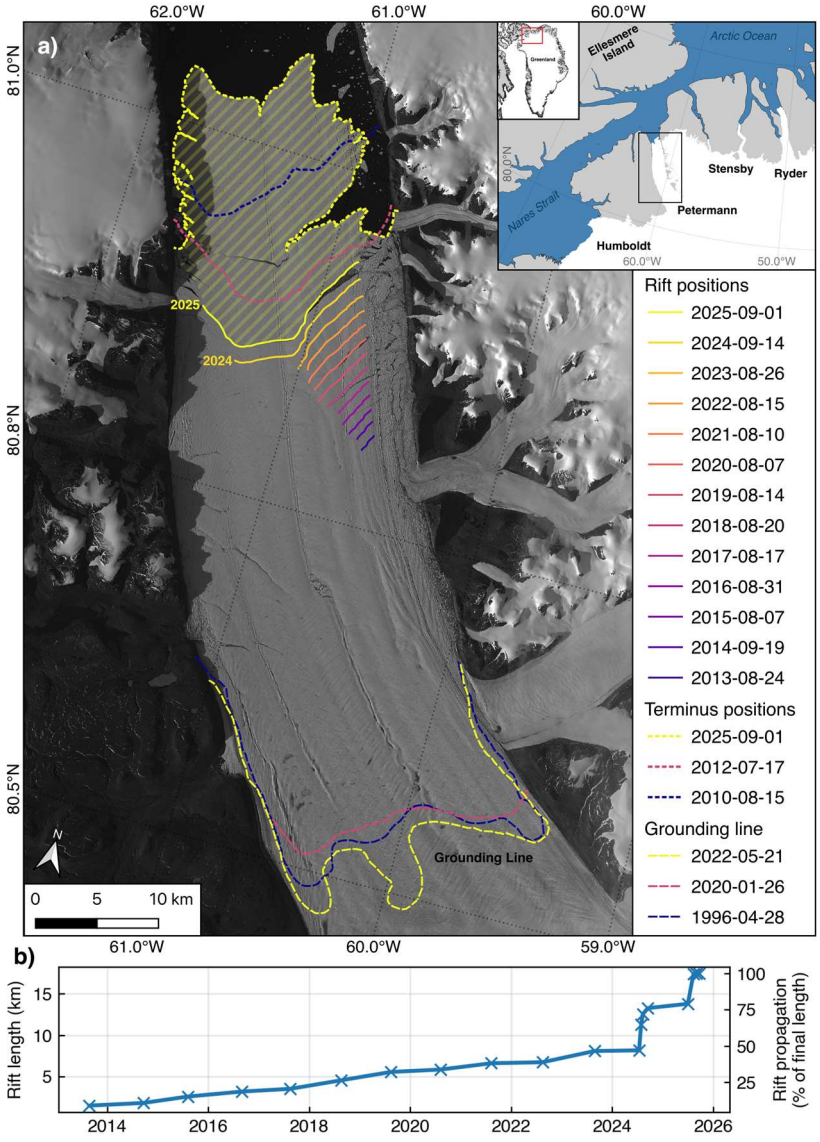
Ice Shelf Rifting and Calving

We map the propagation of two rifts across Petermann Glacier's ice shelf using optical satellite imagery acquired between 2010 and 2026 (Figure 1a and Supplementary Fig. 1a). As of May 2026, both rifts exceeded more than 16 km in length, with an ice bridge less than 500 m in width remaining in each case. Both rifts originated from a similar location on the eastern shear margin and, over time, have propagated towards the western side of the ice shelf (Figure 1a and Supplementary Fig. 1a). We initially observe the first (downstream) rift in 2010, which developed steadily over the following decade, before largely stagnating in 2021 (Supplementary Fig. 1); this rift was previously documented by [51, 52, 56]. In contrast, the upstream rift, which originated three years later in 2013, initially grew slowly, spanning ~8 km (~46% of its total length) by 2023. Following this steady growth, however, the rift then propagated rapidly during the summers of 2024 and 2025; growing by ~3.1 km (~18% of its total length) between 13th–28th July 2024, and ~3.6 km (~21% of its total length) between 1st July–10th August 2025 (Fig 1b). Consequently, the rift now extends to within ~ 400 m of several smaller rifts originating from the western margin of the ice shelf, meaning that only a narrow ice bridge remains intact.

Based on the current rift geometry (Figure 1a), the expected area of ice that will calve is 257 km^2, with 173 km^2 (67%) of ice situated between the downstream rift and the calving front, and a further 84 km^2 between the upstream and downstream rifts. This total area is almost double the size of the area of ice calved during the most recent large calving event in 2012, and the second-largest calving event recorded in the observational

record of Petermann Glacier[34]. Assuming that calving occurs close to the May 2026 upstream rift location, the remaining Petermann Ice Shelf area will be approximately 912 km^2; this would represent a 22% reduction in the current ice shelf area. The new calving front will lie approximately 2.4 km and 11.0 km further inland of its position following the 2012 and 2010 calving events respectively, leaving Petermann Glacier at its most receded position in the observational record[49].

Figure 1: Rift propagation on Petermann Ice Shelf 2013-2025.



a) Propagation of the upstream (initiating in 2013) rift and terminus positions of Petermann Glacier, northwest Greenland. Rift traces mapped between 2013 and 2025 are shown as coloured solid lines. Terminus positions from 2010, 2012, and

2025 are shown as dotted lines, and grounding line positions from 1996, 2020, and 2022 as dashed lines[57]. The hatched area indicates the region of the ice shelf delineated by the current rift geometry and expected to calve. The background image is a Sentinel-2 scene acquired on 31 August 2025. (b) The temporal evolution in the upstream rift length between 2013 and 2025.

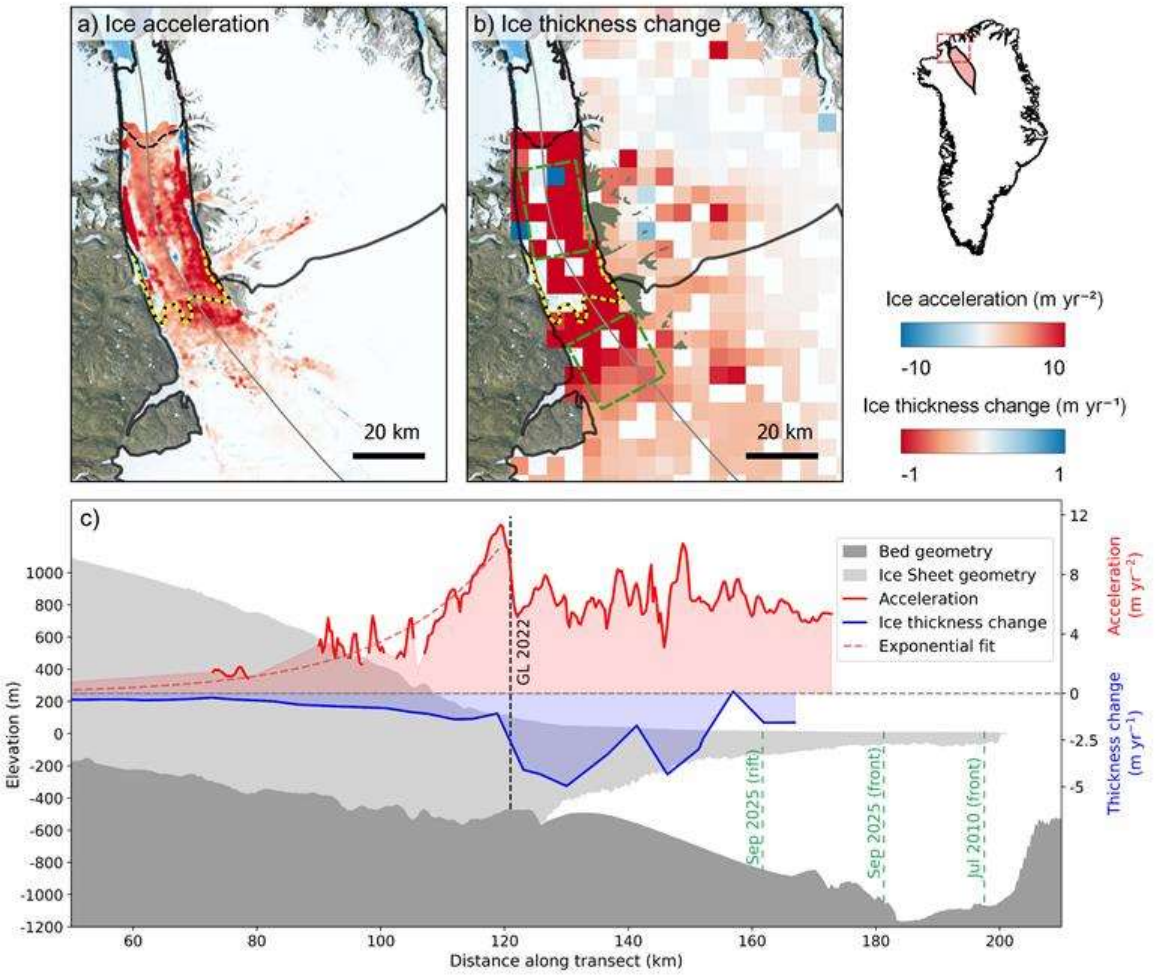
Ice Shelf and Glacier Acceleration

To investigate the dynamic evolution of Petermann Glacier and its ice shelf over the period of rift propagation, we analysed monthly ice velocity measurements derived from the Sentinel-1 satellite, spanning the period from January 2015 to May 2025 (see Methods). Ice velocity time-series were computed within two 400 km^2 regions; one located on the ice shelf and the other further upstream on the grounded portion of the glacier (Figure 2b). Our results show that on average, flow speeds on the ice shelf were approximately 60% higher than those on the grounded ice (1.22 ± 0.08 km yr^{-1} and 0.76 ± 0.10 km yr^{-1}, respectively). Both floating and grounded ice exhibit a pronounced seasonal velocity cycle, with mean summer flow speeds exceeding winter values by 18% and 22% during the study period, respectively.

Given the varying amplitude of seasonal ice acceleration, we estimated the long-term (decadal-scale) change in glacier acceleration by fitting a linear trend to the winter (December-February inclusive) ice velocity measurements. We computed rates of velocity change at each pixel to assess the spatial extent and pattern of ice acceleration. Our measurements show widespread and sustained acceleration across the Petermann Glacier ice shelf during the last decade, at a mean rate of 5.88 ± 1.81 m yr^{-2} over the 10-year period (Figures 2a and 3a). Spatially, the rate of acceleration is observed to peak at approximately 13.0 ± 1.2 m yr^{-2}, 5 km upstream of the 2022

grounding line (Figure 2c). Moving further inland, we find that the rate of acceleration decays approximately exponentially from its peak close to the grounding line, with decadal-scale acceleration still detected more than 50 km upstream of the 2022 grounding-line position (Figure 2c). Our spatially resolved estimates of ice speed change indicate that the two major tributaries flowing into the ice shelf from the eastern side (Figure 2a) also accelerated throughout that period, indicating that the changing dynamics were not limited solely to the main Petermann glacier trunk.

Figure 2: Decadal-scale ice acceleration and thickness change across the Petermann Ice Shelf and Glacier.



Maps of a) winter (DJF) ice flow acceleration derived from Sentinel-1 between 2015 and 2025, and b) rate of ice thickness change derived from CryoSat-2 between 2010 and 2024, with the 2022 grounding line position also shown (yellow and black dashed line[57]).

The solid grey line in (a) and (b) marks the position of the longitudinal profile shown in (c). The dashed green boxes shown in b) indicate the locations of the 400 km^2 analysis regions where we extract ice thickness change and velocity measurements. In a) and b) the basin outline is shown as a solid black line encompassing grounded[58] and floating [1, 59] ice, with the terminus delineation corresponding to the calving front location prior to the 2010 calving event, and the dashed black line the calving front position following the 2012 calving event. The background map in a) and b) is a Google Earth composite image comprising data acquired by Landsat-8 and Sentinel-2 in June 2025. c) shows a longitudinal cross section of the Petermann Glacier and ice shelf (light grey), and its bed (dark grey) extracted from BedMachine v5 [1, 59]. The average 2015-2025 ice acceleration (red line and shading; computed over winter months) is shown along the flowline, along with an exponential fit upstream of the grounding line (dashed red line). The 2010-2024 rate of ice thickness change from CryoSat-2 is also shown along the flowline (blue line and shading). The green dashed lines mark the positions of the calving fronts in September 2025 and July 2010 (prior to the 2010 calving event), along with the location of the upstream rift in September 2025, which is expected to correspond to the post-calving front position.

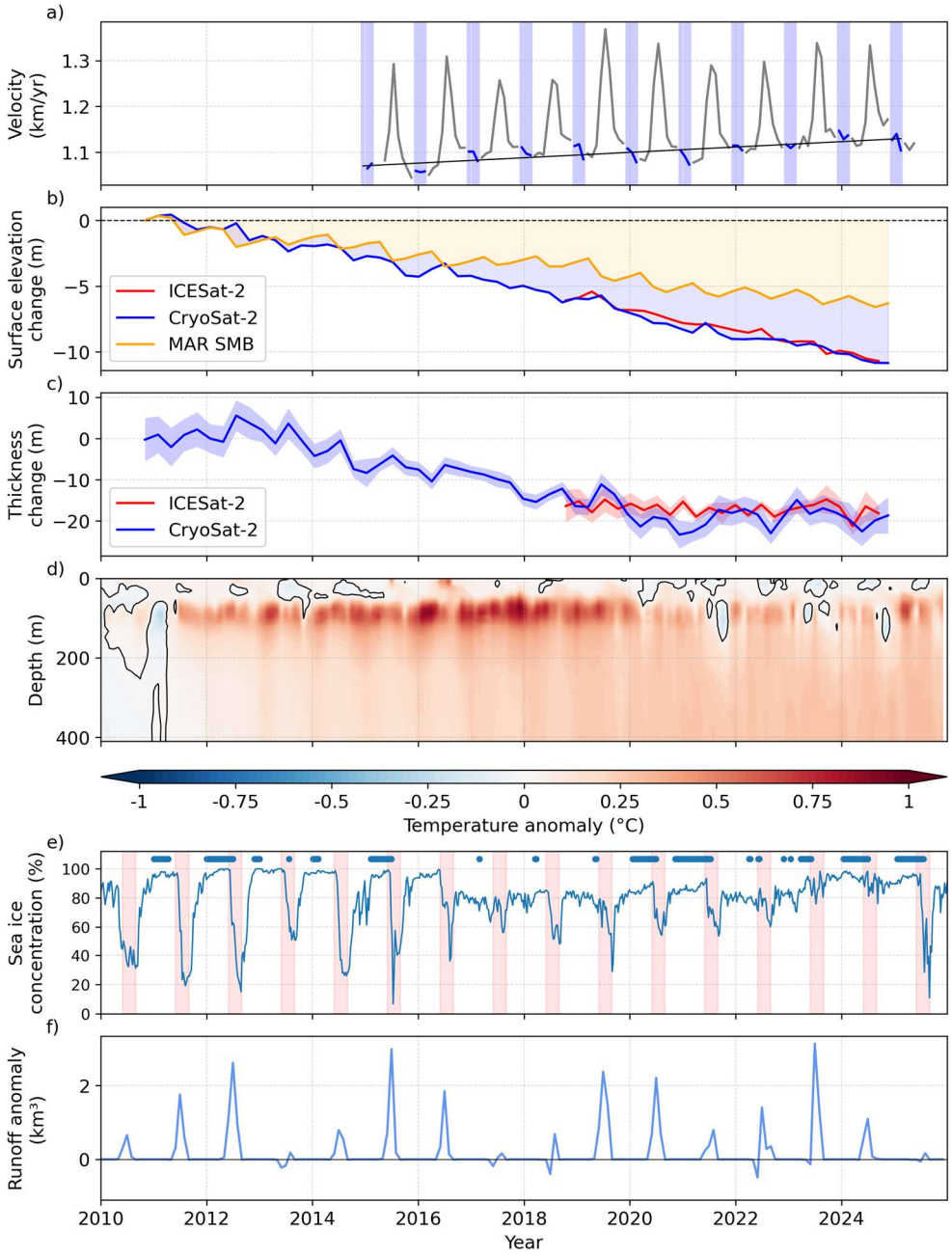
Ice Shelf and Glacier Thinning

We use CryoSat-2 ThEmatic PrOducts (Cryo-TEMPO) Baseline D (ESA, 2025) and ICESat-2 ATL06 Version 6 [60] measurements to derive estimates of ice thickness change over the periods November 2010 to December 2024, and October 2018 to December 2024, respectively. In each case, we compute linear rates of elevation change on a 5 x 5 km grid, together with spatially aggregated time series for the two analysis regions located on Petermann Glacier's ice shelf and the ice immediately upstream of the grounding line (see Methods and Figure 2b). Over the ice shelf, we estimate that the mean rate of thickness change during the CryoSat-2 period was -2.23 ± 0.96 m yr^{-1}, with a maximum observed rate of thinning of 5.46 ± 0.72 m yr^{-1} (Figure 2b). The decrease in ice thickness primarily occurred between July 2012 and September 2020, during which time the ice shelf thinned by a total of 25.16 ± 4.27 m (Figure 3c) over the analysis region; equivalent to an ~11% reduction in its estimated mean thickness[1]. Alongside ice shelf thinning, our analysis also shows sustained thinning upstream of the grounding

line, with the fast-flowing trunk of the glacier having thinned by 10.84 ± 0.66 m since 2010 (Figure 3b). From our CryoSat-2 record, we compute a mean grounded ice thinning rate of -0.82 ± 0.16 m yr^{-1} for the period 2010-2024 (Figure 2c), which is comparable to the rate of -0.80 ± 0.55 m yr^{-1} that we derive from ICESat-2 data for the period 2018-2024.

The observed changes in grounded ice thickness may be caused by surface mass balance or ice dynamical processes [5, 19, 61]. If the decadal-scale acceleration in ice velocity has led to Petermann Glacier entering a state of dynamic imbalance, then the observed rates of ice thinning will exceed those driven by surface melt alone. To assess whether this is the case, and to quantify the relative contribution of dynamical imbalance to the observed elevation changes, we used the Modèle Atmosphérique Régional (MAR) regional climate model [22, 65] to partition the total elevation change into surface mass balance and ice-dynamical imbalance components (Figure 3b). This analysis suggests that almost half (-4.54 ± 1.16 m; ~42%) of the observed elevation change since 2010 immediately upstream of the grounding line is attributable to dynamical imbalance of Petermann Glacier, with the remainder (-6.30 ± 0.95 m) resulting from surface mass imbalance. As such, our observations provide evidence that Petermann Glacier has been in a state of dynamic imbalance throughout the past decade.

Figure 3: Time series of glacier and environmental changes.



a) Mean monthly ice velocity from Sentinel-1 averaged over the ice shelf. A linear trend is fitted to the winter velocities (shaded blue bars and blue lines); b) the dynamic (shaded blue) and surface mass balance (SMB; shaded orange) components of the cumulative surface elevation change observed by Cryosat-2 (blue line) and ICESat-2 (red line) for a 400 km^2 region of the grounded glacier; c) cumulative ice shelf thickness change derived from CryoSat-2 and ICESat-2 (location shown in Figure 2b; green box); d) monthly ocean temperature anomalies from ORAS5 [62] from the mouth of Petermann Fjord (Figure 4) calculated with respect to the monthly 1993-2016 means. The black lines contour the 0°C anomaly; e) landfast sea ice presence[63] (upper blue dots) and sea ice concentration (blue line) from ERA-5 [64] for a location at the mouth of Petermann Fjord. Summer months (JJA) are shaded red; f) Monthly

anomalies in basin runoff relative to the 1980-1995 climatological mean from MAR [22, 65].

Ocean and Atmospheric Change

To investigate possible environmental drivers of the dynamic imbalance at Petermann Glacier, we analysed ocean temperature reanalysis data, sea ice concentration observations, and output from a regional climate model to assess climatic conditions during the study period. We used the European Centre for Medium-Range Weather Forecasts (ECMWF) ORAS5 global ocean reanalysis system[62] to extract ocean temperature estimates for the 410-meter water column at the mouth of Petermann Fjord (location shown in Figure 4). We then computed time-varying ocean temperature anomalies during the period 2010 to 2025, relative to a monthly mean climatology estimated over the historical 1996 to 2016 period (Figure 3d). Our results show that from early 2011 onward, ocean temperatures at the mouth of Petermann Fjord were almost uniformly warmer than the historical mean, with temperatures below a depth of 150 m on average 0.21 °C warmer, and temperatures between 50 and 120 m depth on average 0.33 °C warmer. Within this period, the most notable signal is one of sustained excess warmth in the upper ocean column between 2012 and 2019 (Figure 3d), with the ocean temperature anomaly reaching its peak (0.93 °C warmer than the historical mean) between 2016 and 2019 at depths of 50 to 120 meters. This was followed by another shorter pulse of ocean warmth in 2025, with temperatures approximately 0.67 ° C above the historical mean. These periods of excess ocean warmth would have had the capacity to drive enhanced ocean melting of the ice shelf. Indeed, it is notable that that we observe rapid ice shelf thinning to occur over a similar period (2012-2020) to when warmer ocean waters were present in the fjord (Figure 3c).

Next, we extracted estimates of landfast sea ice presence[63] and sea ice concentration from the ECMWF ERA-5 reanalysis[64, 66] for the same fjord mouth region used for the ocean reanalysis. These data indicate that during the warmest ocean phases, landfast sea ice was largely absent, and autumn, winter and spring sea ice concentration was relatively low. Particularly low winter sea ice concentration and minimal landfast sea ice was observed between 2016-2019, when the warmest ocean temperatures were recorded (Figure 3d-e). Finally, we computed basin-wide surface meltwater runoff anomalies relative to a 1980-1995 climatological baseline, using model output from MARv3.14.3 simulations[22, 65] (Figure 3f). These data indicate that runoff over the past decade has been, on average, higher than the long-term mean, although there is no clear correspondence between periods of high runoff and when the ice shelf thinned most rapidly.

Discussion

Our observations of ice flow acceleration and thinning show that over the past decade Petermann Glacier has been in a state of dynamic imbalance, losing more ice to the ocean than has been replenished over its upstream catchment. Our ice speed measurements show that Petermann Glacier has undergone a modest, yet persistent, acceleration (Figure 3a), which although relatively low in magnitude (up to 13.0 ± 1.2 m yr^{-2}), has now been sustained for a decade, and represents a significant departure from previous decades of perceived stability (e.g. [55, 67, 68]). As a result of this acceleration, more ice has been advected downstream; and our observations show that since 2010, 42% of thinning immediately upstream of the grounding line can be attributed to ice dynamic processes.

On the ice shelf itself, alongside the observed widespread acceleration, we find evidence of significant thinning over the past decade, which was most pronounced between 2012-2020 when the ice shelf lost ~ 11% of its total thickness. This thinning occurred at a time of low landfast sea ice conditions, low autumn, winter and spring sea ice concentration, and anomalously warm ocean temperatures at the mouth of Petermann Fjord. Our measurements therefore provide new observational support for previous modelling studies, which have suggested that the absence or reduction of landfast sea ice may increase ocean temperatures within Petermann Fjord and basal melting of the ice shelf, by allowing greater wind-induced upwelling of warm Atlantic Water into the fjord [42, 46]. This warm water has the capacity to increase basal melting at draft depths of <200 m, which in turn acts to strengthen circulation in the sub-shelf cavity and drive additional heat to the grounding line (~600 m depth)[42]. Additionally, it is interesting to note that low sea ice concentrations have preceded previous Petermann calving events in 2010 and 2012[46], and so the low sea ice concentration recorded in the summer of 2025 (Figure 3e) may increase the probability of Petermann calving its latest large iceberg in 2026.

Although there is a clear temporal correspondence between the period of enhanced ocean warmth and ice shelf thinning, the exact processes driving the observed dynamic imbalance are less clear. Changes in the geometry and structural integrity of the ice shelf both have the potential to drive the observed dynamic imbalance, by reducing the ice shelf's buttressing potential. In this regard, we assess the temporal evolution in the longitudinal gradient of ice shelf velocity, which indicates a progressive switch from flow deceleration (-2.37 ± 0.27 m yr^{-1} km^{-1} between 2007-2012), to acceleration (+0.26 ± 0.24 m yr^{-1} km^{-1} between 2019-2024) (Supplementary Fig. 2). This provides observational

support for the hypothesis that there has indeed been a gradual loss of ice shelf buttressing, which has accompanied the observed acceleration in ice flow and dynamic thinning.

In theory, several different mechanisms could explain this loss of buttressing, including 1) a reduction in basal resistance arising from grounding line retreat, 2) a weakening of the rheological strength of the ice due to increased crevassing across the ice shelf, and 3) a reduction in the resistive stresses imparted by the fjord walls, resulting from changes to the ice shelf geometry. Regarding the first of these processes, recent analysis does indeed indicate a period of grounding line retreat between 2015 and 2018[55], which coincided with our observations of increased ocean temperatures. However, the dynamic imbalance signal that we observe was already evident prior to this period, during a time of apparent grounding line stability[55]. Thus, although the observed grounding line retreat may have contributed to the velocity response in later years, as also noted in a previous study [55], it cannot have served as the initial trigger. Second, a loss of rheological strength resulting from an increase in the number of crevasses on the ice shelf also has the potential to reduce the ice shelf's buttressing potential[69] . However, although a recent Greenland-wide study reports an increase in crevasse volume on Petermann's grounded ice between 2016 and 2021[70], observations of any changes in the number, and volume, of crevasses across the ice shelf itself are lacking. As such, there is currently no evidence to suggest that a progressive increase in crevassing has contributed to the ice shelf's flow acceleration, although better observational datasets are needed, alongside further advances in process understanding of the broader impact of crevassing upon ice shelf stability[71, 69].

Thirdly, a reduction in the buttressing resulting from the lateral resistive stresses imparted by the fjord walls may result from ice shelf thinning, or the mechanical decoupling of downstream ice due to rift propagation and eventual calving[47, 54]. Following the 2010 and 2012 Petermann Ice Shelf calving events, diagnostic modelling suggested that the limited dynamic response observed was a result of the distal ice shelf exerting little resistance to flow. This was due to the calved ice being thin relative to the ice shelf width, rheologically soft, and having only a weak attachment to the sidewalls[47, 54]. In contrast, any changes occurring closer to the grounding line, where the ice is currently thicker and stronger, are expected to exert a greater control upon the ice shelf's buttressing capability[54]. The implications of this are two-fold, (1) that the widespread thinning of floating ice close to the grounding line – as we have observed here since 2010 – may indeed have induced a reduction in buttressing and consequent acceleration in ice flow, and (2) our observations of rift propagation (Figure 1), and the eventual iceberg calving, suggest a continued reduction in the area buffering mechanically stronger ice close to the grounding line[54]. Our observations not only suggest a trajectory towards further acceleration and increased ice discharge in the future, but also point to the underlying complexity and inherent feedbacks within the glacier-ice-shelf-ocean system. This reinforces the need for dedicated modelling studies of Petermann Glacier to better understand the interplay between sea ice, ocean temperatures, the ice shelf and glacier dynamics; and the extent to which increased subglacial discharge may also act to strengthen circulation and melting within the sub-ice shelf cavity[72, 73].

At the regional scale, mass loss from northern sectors of the Greenland Ice Sheet has increased over recent decades, although rates of mass imbalance remain moderate by

comparison to the ice sheet's western and southern margins[5]. At present, the remaining ice shelves in this region play a unique role in restraining discharge from the largest glacier outlets, which together hold a significant sea-level potential[54]. With ocean warming projected to increase over the coming century[74], it is likely that these remaining ice shelves will become increasingly vulnerable to further retreat and collapse, with the associated loss of buttressing expected to drive accelerated sea-level contributions. In this regard, evidence from several large outlet glaciers in northern Greenland suggests that retreat of the calving front close to the grounding line may increase ice discharge by up to 40% over the next two centuries [29, 75]. Our results, which show persistent ice shelf thinning, acceleration and rift propagation over the past decade, provide observational evidence that Petermann Glacier is becoming less stable as its ice shelf progressively recedes and thins. Should this trend continue, Petermann Glacier may become a more significant contributor to Greenland's overall sea-level contribution; a change that, once initiated, would be difficult to reverse[29]. Alongside these terrestrial impacts, increased calving frequency of large, tabular icebergs poses additional risks to the marine environment, including potential disruption to polar operations such as shipping and coastal industries[37, 38, 76]. As vectors of cold, fresh meltwater, icebergs may further influence ocean stratification, ecosystem productivity, sea ice extent, ocean circulation, and deepwater formation[33, 34, 77, 78, 79, 80]. Despite this, iceberg deterioration via fracture remains absent from the most widely-used ocean models, highlighting the need for observational datasets, improved parameterisations, and better integration of iceberg dynamics into the next generation of oceanographic models.

In this study, we have documented the decadal-scale thinning and acceleration of the second largest remaining ice shelf in Greenland. We show that Petermann Ice Shelf is

now poised to calve another large (~250 km^2) iceberg, leaving the new calving front at its most retreated position on record. We observe that the upstream glacier, which extends more than 500 km into the interior of the ice sheet and drains a catchment containing 0.41 m of potential sea-level rise, is exhibiting signs of dynamic imbalance, with sustained acceleration observed upstream of the grounding line and rates of glacier thinning that exceed those expected from surface mass balance alone. Examining ocean reanalysis data, we find that the highest rates of ice shelf thinning occurred at a time when subsurface ocean temperatures were anomalously warm, and the presence of sea ice and landfast ice at the fjord mouth was low. Together, these observations highlight the sensitivity of Petermann Glacier to environmental forcing over the past decade and, more broadly, the complexity in understanding the response of Greenland's marine-terminating glaciers and ice shelves to future climate change. With the imminent calving of another large iceberg from Petermann Glacier, an event that is expected to reduce the size of the remaining ice shelf by almost one quarter, comes the pressing need for coordinated observational and modelling studies to better constrain the future evolution of Greenland's marine-terminating glaciers.

Methods

Rift Formation and Propagation

Rift evolution was quantified using optical satellite imagery acquired between 2010 and 2026, including Landsat 7 (2010–2012), Landsat 8 (2013–2014) and Sentinel-2 (2015 onward). Late-summer scenes (July–September) were preferentially selected to maximise surface visibility and minimise seasonal surface effects. Rift traces were manually digitised from orthorectified imagery based on visible fracture geometry, tonal

contrast, and surface morphology. Each rift was represented as a polyline corresponding to the mapped fracture trace, and cumulative length was measured from a fixed reference origin for each system. Length through time was derived from successive annual observations. The uncertainty associated with rift delineation is primarily governed by image spatial resolution (10–15 m), with additional minor variability introduced during manual digitisation.

Ice Velocity

Ice velocity was measured using a time-series of synthetic aperture radar (SAR) imagery from the Sentinel-1 constellation, part of the European Commission's Copernicus programme and operated by the European Space Agency[81]. We use all available Level-1C interferometric wide mode (IW) single look complex (SLC) images acquired over Petermann Glacier in the horizontal transmit-horizontal receive (HH) polarisation. The data acquisitions cover a decade long period from 2015 to 2025, with all of 6- and 12-day separated image pairs used to measure ice velocity. Image pairs are co-registered and georeferenced using the ArcticDEM v4.1 digital elevation model at 100 m spatial resolution[82] and offset tracking is performed using an intensity feature tracking routine utilising frequency-domain normalised cross-correlation implemented with the GAMMA Remote Sensing software package[79, 83, 84,85]. We repeat the feature tracking routine using three tracking window sizes (256 x 64, 350 x 76, 512 x 128) to maximise coverage. We form an error weighted mean of the three tracking results for each available image pair filtering outliers through comparison to a reference velocity field for speed and flow direction[86] and form monthly mosaics from these data which we use to derive measurements of speed change. A corresponding error is calculated by dividing the

magnitude of the velocity measurement by the signal-to-noise ratio of the cross-correlation calculation[48].

Surface Elevation Change

We derive rates of surface elevation change from radar and laser altimetry acquired by the CryoSat-2 and ICESat-2 satellites. For CryoSat-2, we use the European Space Agency CryoSat-2 ThEmatic PrOducts Baseline-D Level-2 product (CryoTEMPO[87]) spanning the period 2010-2025. For ICESat-2, we use the NASA's ATL06 Land Ice Height product (Release 006[60]), for the period 2018-2025. ICESat-2 ice surface elevation measurements over the Petermann Ice Shelf were corrected for ocean tides and the inverse barometer effect using the parameters provided within ATL06. Corrections for the same geophysical effects are already applied to the CryoSat-2 Cryo-TEMPO product. Both datasets provide geolocated Level-2 elevation measurements along the satellite track. For each mission, observations are gridded on a 5 × 5 km grid, based on a Polar stereographic projection (EPSG: 3413) with a standard parallel of 70°N and a central meridian of 45°W.

Surface elevation change is computed independently for each mission by fitting a spatio-temporal surface model to all elevation measurements within each grid cell, following the approaches described in [88] and [89]. The fit is applied recursively, with measurements deviating by more than 2σ from the model removed at each stage, until all remaining residuals fall within ±2σ, a minimum number of measurements remain in the grid cell, or a maximum number of iterations is reached. For CryoSat-2, we applied a backscatter correction to account for correlated fluctuations in elevation and power, which are associated with the impact of variations in snowpack characteristics upon

the received radar waveform[90, 91]. Gridded elevation change measurements (dh) are aggregated into 90-day epochs by averaging all valid grid-cell solutions within each epoch. We correct for glacial isostatic adjustment using the ICE-5G (VM2) model[92]. Finally, a linear least squares regression is fitted to the 90-day time series to calculate the elevation change rate (dh/dt) per grid-cell. Elevation change uncertainty is calculated as the standard error of elevation change values within each 90-day epoch. Elevation change rate (dh/dt) uncertainty is calculated by summing in quadrature the elevation change uncertainty and the model uncertainty, with the latter defined by the standard error of the estimated slope from the linear regression.

To isolate the dynamic component of the total surface elevation change observed by the altimetry measurements over grounded ice, the surface elevation change arising from surface mass balance processes must be estimated and removed. This is done by computing the deviation of the SMB-driven elevation change from its long-term, climatological mean, which is assumed to represent steady-state conditions[93, 94]. Here, the SMB-driven change in elevation incorporates both the effects of surface mass gain or loss, together with changes in firn air content (FAC). More specifically, for each grid cell, the linear trend in the modelled cumulative SMB and FAC height change is computed over the reference epoch 1980–1995, and then used to detrend the cumulative SMB height change during the full study period. This detrended time series is then subtracted from the altimetry time series, to isolate the dynamic component of the observed elevation change signal[93, 94]. The uncertainty of our dynamical imbalance estimates is calculated by summing in quadrature the elevation change uncertainty and

the regional climate model uncertainty, with the latter assigned a value of 15% of the modelled elevation change.

Over floating ice, elevation change is converted to thickness change under the assumption that floating ice exists in hydrostatic equilibrium (equation 1):

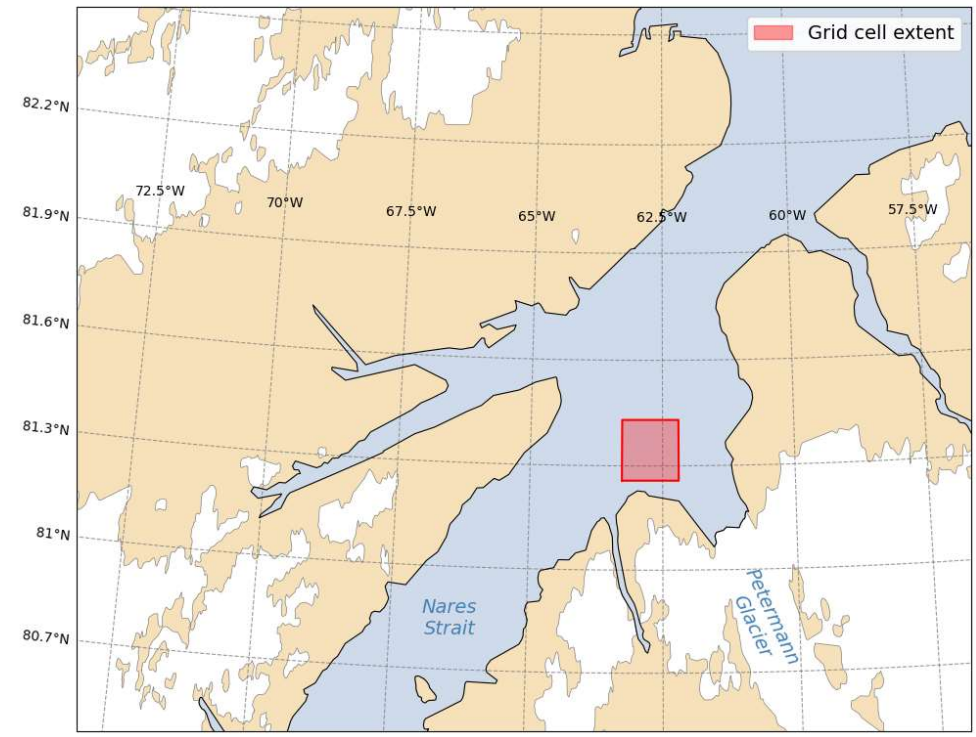
$$dH = dh\ (\rho_w/(\rho_w - \rho_i)) \quad (1)$$

Here, dH is the ice thickness change, dh is surface elevation change, ρ_i is the density of ice (assumed to be 917 kg m^{-3}) and ρ_w is the density of water (assumed to be 1027 kg m^{-3}). After converting to ice thickness change, we account for ice thickness changes due to surface mass balance and firn air compaction by subtracting the combined height change anomalies to account for the steady state signal as described above.

Ocean and Atmosphere Modelling

Ocean temperature anomalies are computed using potential temperature data from the ECMWF Ocean Reanalysis System 5 (ORAS5[62]). ORAS5 provides global coverage of oceanographic variables from 1958 to present at a horizontal resolution of ~0.25° × 0.25° across up to 75 vertical levels spanning 0–5,500 m depth. We extract potential temperature estimates from 1993 to 2025 for a grid cell located at the mouth of Petermann Fjord (Figure 4), retaining all vertical levels to ~410 m — the maximum ocean depth resolved within that grid cell. Monthly climatological means are computed for each depth level over the reference period 1993–2016, and anomalies are derived by subtracting these climatological means from the corresponding monthly potential temperature estimates across the full study period.

Figure 4: Location of the ORAS5 grid cell used to calculate ocean temperature anomalies.



Ice sheet runoff and SMB-related surface height changes are derived from daily simulations produced by the Modèle Atmosphérique Régional (MAR) Regional Climate Model (RCM) [22, 65]. MAR is a coupled surface–atmosphere model forced at its lateral boundaries by reanalysis data; here we use daily MARv3.14.3 simulations over Greenland forced by ERA-5 reanalysis at a horizontal resolution of 5 km. Runoff anomalies for the Petermann Glacier catchment (encompassing grounded and floating ice) are computed by subtracting the monthly climatological means of total basin runoff for the reference period 1980–1995 from the corresponding monthly estimates over the study period.

Sea Ice

Landfast sea ice (LFSI) presence was extracted from weekly regional sea-ice charts produced by the Canadian Ice Service. These charts are composed of polygons that delineate areas of sea ice based upon concentration and ice type. All information concerning sea-ice condition was extracted across available charts between 4 January 2010 and 16 February 2026 for the polygon containing the coordinate 81.37° N, -62.63° W. The presence of LFSI was recorded when the floe size code of 08 or 8 was given, based on the use of SIGRID or egg-code convention, respectively[63]. Sea-ice concentration was extracted daily for this same location and period from the ECMWF Reanalysis v5 (ERA-5), which provides hourly data on a grid with horizontal resolution of 0.25° × 0.25° [64].

Data Availability

The original Copernicus Sentinel-1 and Sentinel-2 data supporting this study can be freely downloaded from the Copernicus Data Space Ecosystem (https://dataspace.copernicus.eu/) or the Alaska Satellite Facility (https://asf.alska.edu). The ECMWF ORAS5 and ERA5 datasets can be freely downloaded from the EU's Copernicus Climate Change Service Climate Data Store (ORAS5: https://cds.climate.copernicus.eu/datasets/reanalysis-oras5?tab=overview, ERA5: https://cds.climate.copernicus.eu/datasets/reanalysis-era5-single-levels?tab=overview). Sea-ice charts are available through the Canadian Ice Service ice archives (https://iceweb1.cis.ec.gc.ca/Archive/page1.xhtml). ERA5 sea-ice concentrations are available via the Copernicus Climate Change Services. Cryo-TEMPO POCA Land Ice Baseline D data are available from https://doi.org/10.5270/CR2-

3205d1e, and can be accessed via the cs2eo data platform at https://cs2eo.org/. ICESat-2 ATL06 Land Ice Height v6 data are available from https://doi.org/10.5067/ATLAS/ATL06.006. Bed and ice geometry data are available from the National Snow and Ice Data Center (NSIDC) (https://nsidc.org/data/idbmg4/versions/5), and the ArcticDEM mosaics are available from the Harvard Dataverse (https://doi.org/10.7910/DVN/3VDC4W). The finalised version of the data generated from the analysis in this study will be made publicly available on the Zenodo repository prior to publication and will have an associated Digital Object Identifier (DOI).

Code Availability

TBC

Acknowledgements

The authors gratefully acknowledge the European Space Agency and the European Commission for the acquisition and availability of Copernicus Sentinel-1 and Sentinel-2 data, the European Space Agency for the acquisition of CryoSat-2 data, the U.S. Geological Survey for the provision of Landsat data and NASA for the acquisition and availability of ICESat-2 data. The Sentinel-1 ice speed measurements were processed on JASMIN, the UK's collaborative data analysis environment (https://www.jasmin.ac.uk). M. M. and J. M. are supported by the UK Natural Environmental Research Council Centre for Polar Observation and Modelling (Grant No. NE/Y006178/1). K. H. B., A. E. H., and M. M. are supported by the ESA ARCTEX project (Contract No. 4000146172/24/I-KE). A. E. H., and B. J. W., are supported by the ESA 5D

Antarctica project (4000146702/24/I-KE). A. E. H., A. J. C. and I. W. are supported by the ARIA Forecasting Tipping Points GIANT project (SCOP-PR01-P028). M. A. H. is funded by the Leeds - York Natural Environment Research Council (NERC) Landscape Award: UKRI1344. A. J. C. is supported by the Royal Society (RG\R1\251361) and Royal Society of Edinburgh Personal Research Fellowship programme. C.W and J. P. are supported by the EPSRC GLOBE project (Grant No. EP/Y02642X/1).

Author Contributions

KHB, MM and AEH designed and led the study. AG and MAH processed the rift dataset, BJW and AEH processed the velocity dataset, CW, KB and JM processed the altimetry dataset, and JP processed the optical time series dataset. KHB analysed the environmental datasets. KHB, KB and AG generated the figures. All authors contributed to writing and discussions developing the manuscript.

Competing Interests Statements

The authors declare no competing interests.

References

[1] Morlighem, M. et al. BedMachine v3: Complete bed topography and ocean bathymetry mapping of Greenland from multibeam echo sounding combined with mass conservation. *Geophys. Res. Lett.* **44,** 11,051–11,061 (2017).

[2] Shepherd, A. et al. A reconciled estimate of ice sheet mass balance. *Science* **338,**1183-1189. (2012).

[3] Otosaka, I. N. et al. Mass balance of the Greenland and Antarctic ice sheets from 1992 to 2020. *Earth Syst. Sci. Data* **15,** 1597–1616 (2023).

[4] van den Broeke, M. et al. On the recent contribution of the Greenland Ice Sheet to sea level change. *Cryosphere* **10,** 1933–1946 (2016).

[5] Mouginot, J., Rignot, E., Bjørk, A. A. & Wood, M. Forty-six years of Greenland Ice Sheet mass balance from 1972 to 2018. *Proc. Natl. Acad. Sci. U.S.A.* **116**, 9239–9244 (2019).

[6] Rantanen, M. et al. The Arctic has warmed nearly four times faster than the globe since 1979. *Commun. Earth Environ.* **3,** 168 (2022).

[7] Fox-Kemper, B. et al. 2021 Ocean, Cryosphere and Sea Level Change. In: Climate Change 2021: The Physical Science Basis. Contribution of Working Group I to the Sixth Assessment Report of the Intergovernmental Panel on Climate Change. Cambridge University Press, Cambridge, United Kingdom and New York, NY, USA, pp. 1211–1362. (2021).

[8] Tedesco, M. et al. Evidence and analysis of 2012 Greenland records from spaceborne observations, a regional climate model and reanalysis data. *Cryosphere* **7,** 615–630 (2013).

[9] Sasgen, I. et al. Return to rapid ice loss in Greenland and record loss in 2019 detected by the GRACE-FO satellites. *Commun. Earth Environ.* **1,** 8. (2020).

[10] Holland, D.M., Thomas, R.H., de Young, B., Ribergaard, M.H. & Lyberth, B. Acceleration of Jakobshavn Isbræ triggered by warm subsurface ocean waters. *Nat. Geosci.* **1,** 659–664 (2008).

[11] Straneo, F. & Heimbach, P. North Atlantic warming and the retreat of Greenland's outlet glaciers. *Nature* **504,** 36–43 (2013).

[12] Roth, A., Straneo, F., Holte, J., Lindeman, M. & Mazloff, M. A dataset for multidisciplinary applications: thirteen years of ocean observations in Sermilik Fjord, Southeast Greenland. *Earth Syst. Sci. Data* **17,** 6025–6048 (2025).

[13] Naakka, T. et al. Polar winter climate change: strong local effects from sea ice loss, widespread consequences from warming seas. *Atmos. Chem. Phys.* **25,** 8127–8148 (2025).

[14] Goelzer, H., et al. The future sea-level contribution of the Greenland ice sheet: a multi-model ensemble study of ISMIP6. *Cryosphere* **14,** 3071-3096 (2020).

[15] Slater, T., Hogg, A.E. & Mottram, R. Ice-sheet losses track high-end sea-level rise projections. *Nat. Clim. Chang.* **10**, 879–881 (2020).

[16] Aschwanden, A., Bartholomaus, T. C., Brinkerhoff, D. J., & Truffer, M. Brief communication: A roadmap towards credible projections of ice sheet contribution to sea level. *Cryosphere* **15,** 5705–5715 (2021).

[17] Pörtner, H.-O., et al. Technical Summary. In: *Climate Change 2022: Impacts, Adaptation, and Vulnerability.* Contribution of Working Group II to the Sixth Assessment Report of the Intergovernmental Panel on Climate Change. Cambridge University Press, Cambridge, UK and New York, NY, USA, pp. 37-118 (2022).

[18] Van den Broeke, M. et al. Partitioning Recent Greenland Mass Loss. *Science.* **326,** 984-986 (2009).

[19] Shepherd, A. et al. Mass balance of the Greenland Ice Sheet from 1992 to 2018. *Nature* **579,** 233–239 (2020).

[20] Catania G. A. et al. Geometric controls on tidewater glacier retreat in central western Greenland. *J. Geophys. Res. Earth Surf.* **123,** 2024–2038 (2018).

[21] King, M. D. et al. Dynamic ice loss from the Greenland Ice Sheet driven by sustained glacier retreat. *Commun. Earth Environ.* **1,** 1 (2020).

[22] Fettweis, X. et al. Reconstructions of the 1900–2015 Greenland ice sheet surface mass balance using the regional climate MAR model. *Cryosphere* **11,** 1015–1033 (2017).

[23] Box, J. E., Fettweis, X., Stroeve, J. C., Tedesco, M., Hall, D. K., & Steffen, K. Greenland ice sheet albedo feedback: thermodynamics and atmospheric drivers. *Cryosphere* **6,** 821–839 (2012).

[24] Catania G.A., Stearns, L. A., Moon, T., Enderlin, E. & Jackson, R. H. Future evolution of Greenland's marine-terminating outlet glaciers. *J. Geophys. Res. Earth Surf.* **125,** e2018JF004873 (2020).

[25] Benn, D. I., Cowton T., Todd J. & Luckman A. Glacier calving in Greenland. *Curr. Clim. Change. Rep.* **3,** 282-290 (2017).

[26] Slater, D.A. & Straneo, F. Submarine melting of glaciers in Greenland amplified by atmospheric warming. *Nat. Geosci.* **15**, 794–799 (2022).

[27] Choi, Y., Morlighem, M., Rignot, E. & Wood, M. Ice dynamics will remain a primary driver of Greenland ice sheet mass loss over the next century. *Commun. Earth Environ.* **2,** 26 (2021).

[28] Wood, M. et al. Ocean forcing drives glacier retreat in Greenland. *Sci. Adv.* **7,** eaba7282 (2021).

[29] Åkesson, H., Morlighem, M., Nilsson, J. Stranne, C. & Jakobsson, M. Petermann ice shelf may not recover after a future breakup. *Nat. Commun.* **13,** 2519 (2022).

[30] Millan, R. et al. Rapid disintegration and weakening of ice shelves in North Greenland. *Nat. Commun.* **14**, 6914 (2023).

[31] Joughin, I., Smith, B.E., Howat, I.M., Scambos, T. & Moon, T. Greenland flow variability from ice-sheet-wide velocity mapping. J. Glaciol. **58,** 15–31 (2012).

[32] Rignot, E., Velicogna, I., van den Broeke, M. R., Monaghan, A. & Lenaerts, J. Acceleration of the contribution of the Greenland and Antarctic ice sheets to sea level rise. *Geophys. Res. Lett.* **38,** L05503 (2011).

[33] Stern, A.A. et al. Wind-driven upwelling around grounded tabular icebergs. *J. Geophys. Res. Oceans* **120,** 5820–5835 (2015).

[34] Crawford, A. J., Mueller, D., Desjardins, L., & Myers, P. G. The aftermath of Petermann Glacier calving events (2008–2012): ice island size distributions and meltwater dispersal. *J. Geophys. Res. Oceans* **123,** 8812–8827 (2018).

[35] Crawford, A. & Mueller, D. Assessing ice island drift patterns, ice island grounding locations, and gridded bathymetry products between Nares Strait and the North Atlantic. *Arctic* ***76,*** 1-13 (2023).

[36] Mueller, D.R., Crawford, A., Copland, L. & Van Wychen, W. Ice Island and Iceberg Fluxes from Canadian High Arctic Sources (Contract Report No. Final Draft Report). Northern Transportation Assessment Initiative, Innovation Policy Branch, Transport Canada, Ottawa. (2013).

[37] Dalton, A. et al. Understanding changes in iceberg–ship coexistence throughout the eastern Canadian Arctic: 2012–2019. *FACETS* **10,** 1–16 (2025).

[38] Fuglem, M., Richard, M., Kennedy, A., King, T., & Cater, N., 2012. Modelling Risks to Offshore Facilities Associated with Ice Islands off Canada's East Coast, in: SNAME 10th International Conference and Exhibition on Performance of Ships and Structures in Ice. Presented at the SNAME 10th International Conference and Exhibition on Performance of Ships and Structures in Ice, SNAME, Banff, Alberta, Canada. (2012).

[39] Rignot, E. & Kanagaratnam, P. Changes in the Velocity Structure of the Greenland Ice Sheet. *Science* **311**, 986-990 (2006).

[40] Ciracì, E., et al. Melt rates in the kilometer-size grounding zone of Petermann Glacier, Greenland, before and during a retreat. *Proc. Natl. Acad. Sci. U.S.A.* **120,** e2220924120 (2023).

[41] Hill, E.A., Gudmundsson, G.H., Carr, J.R., Stokes, C.R., & King, H.M. Twenty-first century response of Petermann Glacier, northwest Greenland to ice shelf loss. *J. Glaciol*. **67,**147-157 (2021).

[42] Prakash, A., Zhou, Q., Hattermann, T. & Kirchner, N. Impact of the Nares Strait sea ice arches on the long-term stability of the Petermann Glacier ice shelf. *Cryosphere* **17,** 5255–5281 (2023).

[43] Rignot, E. & Steffen, K. Channelized bottom melting and stability of floating ice shelves. *Geophys. Res. Lett.* **35,** L02503 (2008).

[44] Münchow, A., Padman, L. & Fricker, H. A. Interannual changes of the floating ice shelf of Petermann Gletscher, North Greenland, from 2000 to 2012. *J. Glaciol*. **60,** 489–499, (2014).

[45] Washam, P., Münchow, A. & Nicholls, K. W. A decade of ocean changes impacting the ice shelf of Petermann Gletscher, Greenland. *J. Phys. Oceanogr.* **48,** 2477-2493 (2018).

[46] Shroyer, E.L., Padman, L., Samelson, R. M., Münchow, A. & Stearns, L. A. Seasonal control of Petermann Gletscher ice-shelf melt by the ocean's response to sea-ice cover in Nares Strait. *J. Glaciol*. **63,** 324-330 (2017).

[47] Nick, F. M. et al. The response of Petermann Glacier, Greenland, to large calving events, and its future stability in the context of atmospheric and oceanic warming. *J. Glaciol*. **58,** 229-239 (2012).

[48] Lemos, A., Shepherd, A., McMillan, M., Hogg, A. E., Hatton, E. & Joughin, I. Ice velocity of Jakobshavn Isbræ, Petermann Glacier, Nioghalvfjerdsfjorden, and Zachariæ Isstrøm, 2015–2017, from Sentinel 1-a/b SAR imagery. *Cryosphere* **12,** 2087–2097 (2018).

[49] Johannessen, O. M., Babiker, M., & Miles, M. W. Unprecedented Retreat in a 50-Year Observational Record for Petermann Glacier, North Greenland. *Atmos. Ocean. Sci. Lett.* **6,** 259–265 (2013).

[50] Falkner, K. K. et al. Context for the Recent Massive Petermann Glacier Calving Event. *EOS Trans. AGU* **92,**117-118 (2011).

[51] Münchow, A., Padman, L., Washam, P. & Nicholls, K. W. The ice shelf of Petermann Gletscher, North Greenland, and its connection to the Arctic and Atlantic Oceans. *Oceanography*, **29**, 84–95 (2016).

[52] Rückamp, M., Neckel, N., Berger, S., Humbert, A. & Helm, V. Calving induced speedup of Petermann glacier. *J. Geophys. Res. Earth Surf.* **124,** 216–228 (2019).

[53] Hogg, A. E., Shepherd, A., Gourmelen, N. & Engdahl, M. Grounding line migration from 1992 to 2011 on Petermann Glacier, North-West Greenland. *J. Glaciol.* **62,** 1104-1114 (2016).

[54] Hill, E. A., Gudmundsson, G. H., Carr, J. R., & Stokes, C. R. Velocity response of Petermann Glacier, northwest Greenland, to past and future calving events. *Cryosphere* **12,** 3907–3921 (2018).

[55] Millan, R. et al. Ongoing grounding line retreat and fracturing initiated at the Petermann Glacier ice shelf, Greenland, after 2016. *Cryosphere* **16,** 3021–3031 (2022).

[56] Dow, C. F. et al. Basal channels drive active surface hydrology and transverse ice shelf fracture. *Sci. Adv.* **4,** eaao7212 (2018).

[57] Ciracì, E., Rignot, E., & Scheuchl, B. Melt rates in the kilometer-size grounding zone of Petermann Glacier, Greenland before and during a retreat. Dryad https://doi.org/10.7280/D1XT4G (2025).

[58] Mouginot, J. & Rignot, E. Glacier catchments/basins for the Greenland Ice Sheet. Dryad. https://doi.org/10.7280/D1WT11 (2019).

[59] Morlighem, M. et al. IceBridge BedMachine Greenland. (IDBMG4, Version 5). [Data Set]. Boulder, Colorado USA. NASA National Snow and Ice Data Center. https://doi.org/10.5067/GMEVBWFLWA7X (2022).

[60] Smith, B. et al. ATLAS/ICESat-2 L3A Land Ice Height. (ATL06, Version 6). National Snow and Ice Data Center. https://doi.org/10.5067/ATLAS/ATL06.006. (2023).

[61] Van den Broeke, M. et al. Partitioning Recent Greenland Mass Loss. *Science.* **326,** 984-986 (2009).

[62] Copernicus Climate Change Service, Climate Data Store. ORAS5 global ocean reanalysis monthly data from 1958 to present. Copernicus Climate Change Service (C3S) Climate Data Store (CDS). 10.24381/cds.67e8eeb7 (2021).

[63] Environment Canada. Canadian Ice Service SIGRID-3 Implementation 2006. Environment Canada, Government of Canada. (2005).

[64] Copernicus Climate Change Service, Climate Data Store. ERA5 hourly data on single levels from 1940 to present. Copernicus Climate Change Service (C3S) Climate Data Store (CDS). 10.24381/cds.adbb2d47 (2023).

[65] Fettweis, X. et al. Estimating the Greenland ice sheet surface mass balance contribution to future sea level rise using the regional atmospheric climate model MAR. *Cryosphere* **7,** 469–489 (2013).

[66] Hersbach, H. et al. The ERA5 global reanalysis. *Q. J. R. Meteorol. Soc.* **146**, 1999–2049 (2020).

[67] Moon, T. A., Gardner, A. S., Csatho, B., Parmuzin, I. & Fahnestock, M. A. Rapid reconfiguration of the Greenland Ice Sheet coastal margin. *J. Geophys. Res. Earth Surf.* **125,** e2020JF005585 (2020).

[68] Williams, J.J., Gourmelen, N. & Nienow P. Complex multi-decadal ice dynamical change inland of marine-terminating glaciers on the Greenland Ice Sheet. *J. Glaciol*. **67,** 833-846 (2021).

[69] Surawy-Stepney, T., Hogg, A.E., Cornford, S.L. & Davison, B. Episodic dynamic change linked to damage on the Thwaites Glacier Ice Tongue. *Nat. Geosci.* **16**, 37–43 (2023).

[70] Chudley, T.R., Howat, I. M., King, M.D. & MacKie, E. J. Increased crevassing across accelerating Greenland Ice Sheet margins. *Nat. Geosci.* **18,** 148-153 (2025).

[71] Izeboud, M., Wouters, B., de Roda Husman, S. Lhermitte, S. Damage development on Antarctic ice shelves sensitive to climate warming. *Nat. Clim. Chang.* **15**, 1333–1339 (2025).

[72] Washam, P., Münchow, A. & Nicholls, K. W. A decade of ocean changes impacting the ice shelf of Petermann Gletscher, Greenland. *J. Phys. Oceanogr.* **48,** 2477-2493 (2018).

[73] Prakash, A., Zhou, Q., Hattermann, T. & Kirchner, N. Enhanced subglacial discharge amplifies Petermann Ice Shelf melting when ocean thermal forcing saturates. *Nat. Commun.* **16**, 4213 (2025).

[74] Slater, D. A. et al. Twenty-first century ocean forcing of the Greenland ice sheet for modelling of sea level contribution. *Cryosphere* **14,** 985–1008 (2020).

[75] Humbert, A. et al. Precursor of disintegration of Greenland's largest floating ice tongue. *Cryosphere* **17,** 2851–2870 (2023).

[76] Crawford, A. et al. Journey of an Arctic ice island. *Oceanography* **29,** 254-263 (2016).

[77] Smith, K.L. Free-drifting icebergs in the Southern Ocean: An overview. *Deep Sea Res. Part II* **58,** 1277–1284 (2011).

[78] Merino, N. et al. Antarctic icebergs melt over the Southern Ocean: Climatology and impact on sea ice. *Ocean Model.* **104,** 99–110 (2016).

[79] Davison, B.J. et al. Sea level rise from West Antarctic mass loss significantly modified by large snowfall anomalies. *Nat. Commun.* **14,** 1479 (2023).

[80] Zhang, J., Zhang, X., King, M.A. & Lyu, K. The response of the Southern Ocean to Climatological iceberg freshwater forcing. *Clim. Dyn.* **63,** 440 (2025).

[81] Geudtner, D., Torres, R., Snoeij, P., Davidson, M. & Rommen, B. Sentinel-1 System capabilities and applications.*2014 IEEE Geoscience and Remote Sensing Symposium*. 1457–1460 (2014).

[82] Porter, C. et al. ArcticDEM - Mosaics, Version 4.1. Harvard Dataverse. https://doi.org/10.7910/DVN/3VDC4W (2023).

[83] Strozzi, T., Luckman, A., Murray, T. & Wegmuller, U. Glacier motion estimation using SAR offset-tracking procedures. *IEEE Trans. Geosci. Remote Sens.* **40,** 2384–2391 (2002).

[84] Hogg, A. E. et al. Increased ice flow in Western Palmer Land linked to ocean melting, *Geophys. Res. Lett.* **44,** 4159–4167 (2017).

[85] Selley, H.L. et al. Widespread increase in dynamic imbalance in the Getz region of Antarctica from 1994 to 2018. *Nat. Commun.* **12,** 1133 (2021).

[86] Wuite, J., Nagler, T., Hetzenecker, M. & Rott, H. Ten years of polar ice velocity mapping using Copernicus Sentinel-1. *Remote Sens. Environ.* **332,** 115092 (2026).

[87] European Space Agency. Cryo-TEMPO Land Ice, Baseline D. CS2EO Platform https://doi.org/10.5270/CR2-3205d1e (2022).

[88] McMillan, M. et al. Increased ice losses from Antarctica detected by CryoSat-2. *Geophys. Res. Lett.* **41,** 3899–3905 (2014).

[89] Ravinder, N., Shepherd, A., Otosaka, I., Slater, T., Muir, A. & Gilbert, L. Greenland Ice Sheet elevation change from CryoSat-2 and ICESat-2. *Geophys. Res. Lett.* **51,** e2024GL110822 (2024).

[90] McMillan, M. et al. A high-resolution record of Greenland mass balance. *Geophys. Res. Lett.* **43,** 7002–7010 (2016).

[91] Slater, T. et al. A new digital elevation model of Antarctica derived from CryoSat-2 altimetry. *Cryosphere* **12,** 1551–1562 (2018).

[92] Peltier, W. R. Global glacial isostasy and the surface of the ice-age earth: The ICE-5G (VM2) model and GRACE. *Annu. Rev. Earth Planet. Sci*. **32,** 111-149 (2004).

[93] Slater, T. *et al.* Increased variability in Greenland Ice Sheet runoff from satellite observations. *Nat. Commun*. **12**, 6069 (2021).

[94] Smith, B. E. et al. Evaluating Greenland surface-mass-balance and firn-densification data using ICESat-2 altimetry. *Cryosphere* **17,** 789–808 (2023).

Supplementary Files

This is a list of supplementary files associated with this preprint. Click to download.

- PetermannSOMv00.pdf
- timelapsepetermannsceneratenrt001cct50.mp4
- Supplementarymaterialsv01.docx